Research in Pharmaceutical Sciences, February 2026; 21(1): 64-76
Received: 27-04-2024
Peer Reviewed: 30-07-2024
Revised: 30-09-2024
Accepted: 29-10-2024
Published: 26-12-2025

School of Pharmacy & Pharmaceutical Sciences
Isfahan University of Medical Sciences

Original Article

Experimental and theoretical evaluation of antioxidant capacity of flavone glycosides extracted from *Cleome turkmena* Bobrov

Mehrdad Mohammadpour Dehkordi[1], Elham Elahi[2], Samin Mousavi[2], Sara Abdeyazdan[2], and Mustafa Ghanadian[2,*]

[1]*Department of Medicinal Chemistry, Pharmaceutical Sciences Research Center, School of Pharmacy and Pharmaceutical Sciences, Isfahan University of Medical Sciences, Isfahan, I.R. Iran.*
[2]*Department of Pharmacognosy, Pharmaceutical Sciences Research Center, School of Pharmacy and Pharmaceutical Sciences, Isfahan University of Medical Sciences, Isfahan, I.R. Iran.*

Abstract

Background and purpose: In traditional medicine, species of *Cleome* (known in Persian as alaf-e-mar) are used to treat wounds and earaches, as well as for their antihelmintic, carminative, and anti-arthritic properties. Flavonoids, among the most significant phytochemicals in this family, hold pharmacological importance, mainly due to their ability to scavenge free radicals.

Experimental approach: *Cleome turkmena* Bobrov was collected and extracted in methanol. Compounds were isolated by open-column and size-exclusion chromatography. Free radical scavenging ability and reduction potential of isolated flavonols along with allantoin were determined according to the scavenging of the DPPH (diphenyl-picrylhydrazyl) radical and reducing power of Fe^{3+} assays. A theoretical study of their antioxidant capacity was done using density functional theory calculations.

Findings/Results: Allantoin (compound 1), 2 known flavonol glycosides (compounds 2, 4), and 1 undescribed flavonol glycoside (compound 3) were isolated, and their structures were identified using different spectroscopic techniques for the first time in this plant. Among them, compound 4, quercitin-3-O-β-D-glucoside-7-O-α-L-rhamnoside, exhibited the best free radical scavenging and reducing power effects compared to the standards.

Conclusion and implications: All flavone glycosides isolated from *Cleome turkmena* Bobrov showed favorable DPPH radical scavenging and Fe^{3+} reducing power.

Keywords: *Cleome turkmena* Bobrov; Density functional theory; Flavonoids; Quercetin; Radical scavenging.

INTRODUCTION

Cleome, from the Cleomaceae family, is known for its unpleasant smell and taste. It grows in warm regions and comprises approximately 600 species, with 17 species being native to Iran (1,2). Various species of *Cleome* have been utilized in traditional medicine for their medicinal properties, such as being antihelmintic, carminative, anti-arthritic, and useful in wound treatment. *Cleome* phytochemicals showed various biological activities, like antioxidant and wound-healing properties (3,4). Additionally, they are consumed as vegetables, with their leaves and shoots possessing a pungent mustard-like flavor (5). The main phytochemicals derived from this genus are flavonoids (6). Cembranoid diterpenes, triterpenoids, and sesquiterpenes are also found in this genus (3,7). Among all these bioactive compounds, phenolic compounds-specifically flavonoids and flavonol glycosides, are more abundant and hold greater pharmacological importance than the others (8).

*Corresponding author: M. Ghanadian
Tel: +98-3137927125, Fax: +98-3136680011
Email: ghannadian@gmail.com

Access this article online

Website: http://rps.mui.ac.ir

DOI: 10.4103/RPS.RPS_266_23

Quercetin, kaempferol, myricitrin, and rutin are the most common flavonoids found in these plants, along with their derivatives (2,9,10). Flavonoids exist in either glycoside or aglycone forms, although glycoside forms are more prevalent (11). As a subcategory of flavonoids, flavonols help reduce the risk of cardiovascular events (12). Many of the pharmacological effects of flavonols are attributed to their ability to scavenge free radicals (13). In the context, quercetin is a powerful agent that neutralizes superoxide radicals. How it is dosed, processed, and stored plays a crucial role in preserving its antioxidant capabilities, which influences the effectiveness of quercetin in preventing and treating various diseases (14). Kaempferol is similar to quercetin and possesses only one hydroxy group on ring B, recognized as a potent anti-cancer agent by eliminating reactive nitrogen and oxygen species and inhibiting key intracellular components like nuclear factor kappa B (NF-κB), mitogen-activated protein kinases (MAPKs), cyclooxygenase-2 (COX-2), and sirtuin 1 (SIRT1) (15). Myricetin, a simple flavonol, possesses 3 hydroxy groups on ring B and has antioxidant properties that enhance the antioxidant status in cancer cells, protecting against cancer. Additionally, it reduces inflammatory cytokines linked to tissue damage in myocardial dysfunction (16).

Reactive oxygen species (ROS) and free radicals are generated simultaneously during oxidative metabolic processes within the body, playing crucial roles in various physiological functions, such as cell signaling, immunity, redox regulation, tissue balance, and defense against infections. Phenolic antioxidants, known for their effectiveness in neutralizing free radicals and mitigating their harmful effects, find applications in both commercial and biological fields. Density functional theory (DFT) is based on the concept that the total energy of a system can be expressed as a function of electron density. DFT has gained popularity for its speed, accuracy, and applicability to large systems in calculating molecular properties (17-19). Antioxidants can alleviate the detrimental impact of free radicals through mechanisms such as single electron transfer followed by proton transfer (SET-PT), hydrogen atom transfer (HAT), and sequential proton loss electron transfer (SPLET). The DFT approach involves analyzing the energies of the highest-occupied molecular orbital (HOMO) and the lowest-unoccupied molecular orbital (LUMO) (20,21).

Many pharmacological effects of the *Cleome* genus are attributed mainly to flavonols. Since many plants in this genus have culinary applications, investigating their flavonoid content can provide valuable insights for phytochemical studies (7,22,23). Accordingly, this study was conducted to identify the structure of the isolated flavone glycosides extracted from *Cleome turkmena* Bobrov. Subsequently, their free radical scavenging effects were investigated experimentally. Finally, a comparative theoretical study was conducted using DFT calculations to explore their antioxidant properties and mechanisms of action.

MATERIALS AND METHODS

Experimental materials and methods

Plant material

Cleome turkmena Bobrov was collected in August 2013 from Chahchaheh (36°38′N 60°19′E, altitude 495 m), Northern Khorasan, Iran. The plant was identified by Dr. Mohammad Reza Joharchi with voucher specimen Number 3393.

General experiments and procedures

Column chromatography was conducted using Lichroperp RP-18 (25-40 µm, Merck) and Sephadex-LH (Pharmacia in Uppsala, Sweden).To prepare Sephadex LH-20, it was swollen in methanol and packed into a 45 cm long glass column with a 2 cm inner diameter, equipped with a Teflon stopcock, and then flushed with the same solvent at a 3 cm/h flow rate. Thin layer chromatography (TLC) mobile phase consists of CHCl3:MeOH:acetic acid (77:20:3), along with ceric sulfate-sulfuric acid reagent and a natural product reagent (1% methanolic diphenylboric acid-ß-ethylamino ester). Computational analysis was carried out using Hyperchem v07 and Gaussian 09 software packages. ^{1}H NMR and ^{13}C NMR were taken at 400 and 100 MHz, respectively, using DMSO-d6.

Extraction and isolation

The dried aerial parts of plant material (4.0 kg) were crushed, pulverized, and extracted by methanol in a percolator at 3.6 mL/min for 72 h. After filtration, the extract was concentrated and subjected to reverse chromatography using ethanol:water (fraction-1: 10:90; fraction-2: 30:70; fraction-3: 70:30; fraction-4: 100:0) as mobile phase. The fraction-1 contained sugar and salt, as well as fraction-2. The fraction-3 contained nonpolar constituents, which were put aside without any workup. The fraction-2 contained polar components chromatographed on a normal column using $CHCl_3$:MeOH:acetic acid (fraction-2-1:80:10:0; fraction-2-2:80:20:0; fraction-2-3:70:30:0; fraction-2-4:69:30:1; fraction-2-5:65:30:5). TLC profile developed using $CHCl_3$:MeOH:acetic acid (77:20:3) as mobile phase. Reagents used for TLC development were ceric sulfate-sulfuric acid reagent and natural product reagent (1% methanolic diphenylboric acid-ß-ethylamino ester). Spots with yellow color in TLC of fractions 2-2, 2-3, and 2-5 contained flavonoid content. They were further subjected to a polyamide SC6 column using a stepwise gradient of methanol:water (40:60; 75:25; 50:50; 75:25; 75:25; 100:0) as mobile phase. Based on the mentioned TLC profile, the flavonoid subfractions were purified further on the Sephadex LH-20 column (2 × 45) using methanol as the mobile phase. Finally, fractions 3a2 (8.9 mg), 2e4 (15.1 mg), 5d1 (8.3 mg), and 5d2 (6.8 mg) were sent for spectrophotometric methods.

Diphenyl-picrylhydrazyl radical scavenging assay

It was assessed for its scavenging ability by transferring a hydrogen atom to a diphenyl-picrylhydrazyl (DPPH) radical structure following previously established methods (24,25). In summary, 70 µL of a 1 mM methanolic solution of DPPH was combined with 20 µL of various concentrations of samples and ascorbic acid, which served as the positive control (at the concentrations of 1, 10, 25, 50, 100, and 200 µg/mL), in a 96-well plate. Methanol was then added to achieve a total volume of 0.20 mL. After 30 min, the absorbance was measured at 517 nm. The radical scavenging activity was quantified as the percentage of inhibition using equation (1):

$$inhibition\ (\%) = \left(\frac{(Ac - As)}{Ac}\right) \times 100 \qquad (1)$$

where, "Ac" represents the absorbance of the control (blank), and "As" represents the absorbance of the samples. The EC50 value indicates the sample concentration required to 50% scavenge of DPPH free radicals.

Reducing power assay

The capacity of compounds to reduce Fe^{3+} was examined following the procedure outlined by Salmanian *et al*. (25). In summary, various concentrations of the samples (1, 10, 25, 50, 100, and 200 µg/mL), 50 µL of phosphate buffer (0.2 M, pH 6.6), and 50 µL of potassium ferricyanide (1% W/V) were combined in a 96-well plate and incubated at 50 ºC for 30 min. Subsequently, 50 µL of trichloroacetic acid (10% V/V) was added, followed by 50 µL of deionized water containing Tween 80 (5% V/V) and 10 µL of ferric chloride (0.1% W/V). The absorbance was then measured at 700 nm. The reducing power was calculated using equation (2):

$$Reducing\ power\ (\%) = \left(\frac{As}{Ac}\right) \times 100 \qquad (2)$$

where, "Ac" represents the absorbance of the control (blank), and "As" represents the absorbance of the samples (25).

Computational methods

The electron densities of the confirmed structures 2, 3, and 4 were determined using the DFT employing the B3LYP (Becke, 3-parameter, Lee-Yang-Parr) (26). The molecular structures of the compounds under investigation, along with free radicals, anions, or related radical cations, were all optimized using DFT with the B3LYP functional and the 6-311++G** basis set in the Gaussian 03 W program while accounting for water solvent effects. Various electronic properties were computed using frontier orbital theory. Using Koopman's theorem, the first ionization potential (IP) of a molecular system could be estimated as the negative value of the HOMO energy, allowing for the determination of the electron affinity (EA) as the LUMO energy of the system. Parameters such as hardness, IP, EA, and softness were derived using equations 1-10 previously outlined (26).

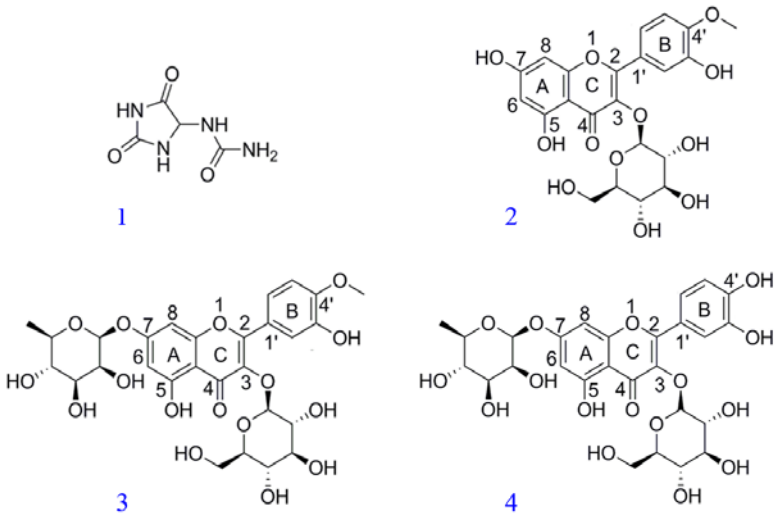

Fig. 1. Structure of compounds studied.

Antioxidant capacity

The phenolic hydroxy groups exhibit their antioxidant capacity primarily through HAT, SET-PT, and SPLET mechanisms. The bond dissociation enthalpy (BDE), along with HAT, IP, proton dissociation enthalpy (PDE) related to SET-PT, and electron transfer enthalpy (ETE) and proton affinity (PA) for SPLET, were computed using equations 1-10 as detailed in previous literature based on the electronic and thermal enthalpies of the involved compounds. Furthermore, spin density distribution analysis was utilized to evaluate the free radical scavenging potential, where a higher delocalization of spin density indicates easier radical formation (27). The structure of the studied compounds and their corresponding numbering system is depicted in Fig. 1, where the glycoside substituent on the C3 or C7 positions of the flavonol ring was replaced by a methyl group for computational simplification.

RESULTS

Spectral data of isolated compounds

Compound 1: allantoin

Amorphous white powder, UV (MeOH, nm) λmax: 205, 254; IR (NaCl) 3419, 3356, 1726, 1666, 1535, 1421, 1180, 1012 cm^{-1}. δ_H 5.22 (d, *J* = 8.4 Hz, H-4), 6.96 (d, *J* = 8.4 Hz, 4-NH-CO), 5.81 (2H, s, 6-NH_2), 8.04 (m, NH-1), 10.9 (NH-3). δ_C 173.0 (C6), 156.8(C5), 156.2 (C2), 61.8(C4). Positive ESI Mass *m/z* 159 $[M+H]^+$.

Compound 2: 4'-O-methylquercetin-3-O-β-D-glucopyranoside

A pale-yellow powder; UV (MeOH, nm) λmax: 257, 355. δ_H 3.12-3.83 (overlapping signals for H-2″, H-3″, H-4″, H-5″), 3.83 (3H, singlet, MeO), 5.56 (doublet, J = 7.6 Hz, H-1″), 6.20 (doublet, J = 2.0 Hz, H-6), 6.44 (doublet, J = 2.0 Hz, H-8), 6.91 (doublet, J = 8.4 Hz, H-5′), 7.48 (doublet of doublets, J = 8.4, 2.0 Hz, H-6′), 7.94 (doublet, J = 2.0 Hz, H-2'); δ_C 56.1 (MeO), 61.0 (C6″), 70.2 (C5″), 74.8 (C4″), 76.8 (C3″), 77.9 (C2″), 94.2 (C8), 99.2 (C6), 101.2 (C1″), 104.4 (C10), 113.9 (C2′), 115.7 (C5′), 121.5 (C1′), 122.5 (C6′), 133.4 (C3), 147.3 (C4′), 149.9 (C3′), 156.7 (C2), 156.9 (C9), 161.7 (C5), 164.8 (C7), 177.8 (C4). Negative ion ESI at 477 $[M-H]^-$, 447 $[M-MeO]^-$, and 315 [M-Glucosyl

Compound 3: 4'-O-methylquercetin-3-O-β-D-glucopyranoside-7-O-α-L-rhamnopyranoside

A pale-yellow powder; UV (MeOH, nm) λmax: 255, 351. δ^H 1.11 (doublet, J = 6.4, H-6‴), 3.12-5.20 (overlapping signals for H-2″-H-6″ and H-2‴-H-5‴), 3.87 (3H, singlet, MeO), 5.56 (broad singlet, H-1‴), 5.59 (doublet, J = 7.8, H-1″), 6.45 (doublet, J = 2.2 Hz, H-6), 6.85 (doublet, J = 2.2 Hz, H-8), 6.92 (doublet, J = 8.4 Hz, H-5′), 7.55 (doublet of doublets, J = 8.4, 2.0 Hz, H-6′), 7.95 (doublet, J = 2.0 Hz, H-2'); δ_C 17.9 (C6‴), 60.5 (C6″), 55.6 (MeO), 69.6 (C5‴), 69.8 (C3‴), 70.0 (C2‴), 70.2 (C5″), 71.5 (C4‴), 74.3 (C4″), 76.3 (C3″), 77.5 (C2″), 94.6 (C8), 98.2 (C1‴), 99.3 (C6),

100.6 (C1″), 105.6 (C10), 113.4 (C2′), 115.1 (C5′), 120.9 (C6′), 122.2 (C1′), 133.2 (C3), 146.9 (C4′), 149.5 (C3′), 155.9 (C2), 156.8 (C9), 160.8 (C5), 161.5 (C7), 177.5 (C4). Negative ESI mass at 623 $[M-H]^-$, 593 $[M-MeO]^-$, 477 [M-rhamnosyl]$^-$, 325, and 316.

Compound 4: quercitin-3-O-β-D-glucopyranside-7-O-α-L-rhamnopyranoside

A pale-yellow powder; UV (MeOH, nm) λmax: 257, 356. δ_H 1.11 (doublet, J = 6.0, H-6‴), 3.08-5.20 (overlapping signals for H-2″-H-6″ and H-2‴-H-5‴), 5.48 (doublet, J = 7.2, H-1″), 5.55 (broad singlet, H-1‴), 6.43 (d, *J* = 2.0 Hz, H-6), 6.79 (d, *J* = 2.0 Hz, H-8), 6.85 (d, *J* = 8.8 Hz, H-5′), 7.60 (2H, overlapped, H-6′, H-2′); δ_C 17.9 (C6‴), 60.9 (C6″), 69.8 (C5‴), 69.9 (C3‴), 70.0 (C2‴), 70.1 (C5″), 71.5 (C4‴), 74.0 (C4″), 76.4 (C3″), 77.6 (C2″), 94.2 (C8), 98.3 (C1‴), 99.3 (C6), 100.6 (C1″), 105.6 (C10), 115.2 (C2′), 116.2 (C5′), 121.0 (C6′), 121.7 (C1′), 133.5 (C3), 144.8 (C4′), 148.6 (C3′), 155.9 (C2), 156.6 (C9), 160.8 (C5), 161.5 (C7), 177.5 (C4). Negative ESI mass: 609 $[M-H]^-$.

DPPH radical scavenging activity

In this test, the reduction in absorbance value and the color shift from purple to yellow signified the conversion of the radical form (DPPH•) to neutral DPPH. The percentage of DPPH scavenging activity exhibited by compounds 1-4 isolated from *C. turkmena* across concentrations of 1.0 to 200.0 µg/mL is illustrated in Fig. 2A.

The EC50 values (µg/mL) derived from the curves depicted in Fig. 2A are compiled in Table 1. Data showed that the inhibition potential of DPPH radical by isolated compounds 1-4 was in the following order: 4 > 2 > 3 > ascorbic acid > 1. Therefore, the antioxidant potential of compounds 2 and 4 was found to be better than ascorbic acid.

Reducing power activity

Figure 2B represents reducing power activities of isolated compounds 1-4 from *C. turkmena* in the concentration range of 1.0-200.0 µg/mL. The ranking order for reducing power was 4 > 3 > 2 > quercetin > 1. The EC_{50} value of reduction power for quercetin was 50.06 µg/mL (28) (Table 2).

DFT calculation results

The calculated HOMO and LUMO energies of compounds 2-4, obtained using the B3LYP/6-311G** level in the polarizable continuum model (PCM), are presented in Table 3. The energy of the HOMO orbital (EHOMO) is commonly regarded as a reliable indicator of scavenging activity. A less negative EHOMO value, approaching zero, suggests higher compound instability and an increased likelihood of electron dissociation. Despite the similar EHOMO values observed across the compounds under investigation, the energy gap (Egap) between EHOMO and ELUMO was also considered to assess the propensity for electron loss and the formation of a radical state.

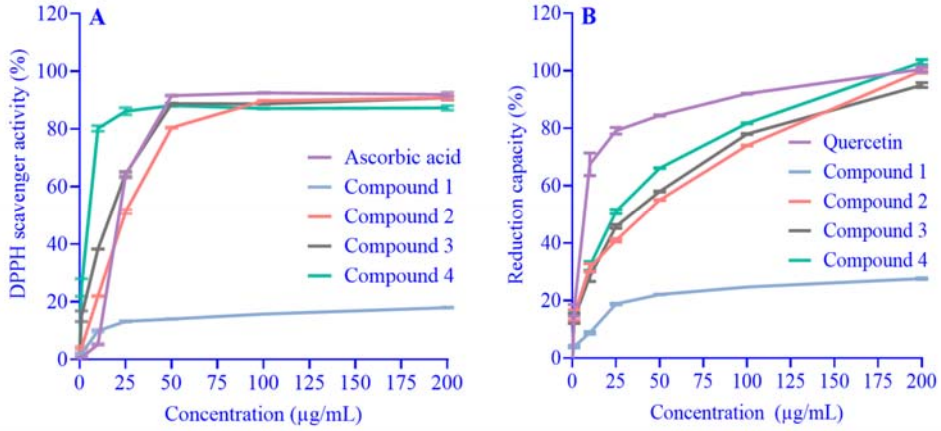

Fig. 2. Antioxidant activities of isolated compounds from *Cleome turkmena* Bobrov. Data were expressed as mean ± SD. (A) DPPH radical scavenging activity and (B) reducing power. DPPH, Diphenyl-picrylhydrazyl.

Table 1. EC_{50} of DPPH scavenging activity of studied structures. Data were expressed as mean ± SD.

Compound	1	2	3	4	Ascorbic acid
EC_{50} (µg/mL)	> 200	15.12 ± 0.64	18.65 ± 1.10	4.50 ± 0.84	19.51 ± 0.14

EC_{50}, Half-maximal effective concentration.

Table 2. EC_{50} of reducing power activity of the studied structures. Data were expressed as mean ± SD.

Compound	1	2	3	4	Quercetin
EC_{50} (µg/mL)	> 200	35.07 ± 2.31	28.21 ± 1.62	18.47 ± 1.21	50.06

EC_{50}, Half-maximal effective concentration.

Table 3. HOMO and LUMO energy, energy gap, and other descriptors calculated at 298.15 K, PCM, B3LYP/6-311+ +G** level of theory (eV), IP, EA, µ, η, and S.

Structure	E_{HOMO}	E_{LUMO}	E_{gap}	IP	EA	η	µ	S
2	-6.107	-2.250	3.860	6.106	2.249	1.929	-4.178	0.260
3	-6.230	-2.317	3.912	6.230	2.317	1.956	-4.273	0.255
4	-6.136	-2.254	3.882	6.136	2.254	1.941	-4.195	0.257

E, Energy; HOMO, highest-occupied molecular orbital; LUMO, lowest-unoccupied molecular orbital; IP, ionization potential; EA, electron affinity; µ, electronic chemical potential; η, hardness; S, softness.

Table 4. Calculated energies of different steps of possible mechanisms of scavenging activity (kJ/mol, at 298.15 K, PCM, B3LYP/6-311+ +G** level of theory).

Structure	Substituent	BDE	IP	PDE	PA	ETE
2	7-OH	362.72	535.70	72.51	139.10	469.11
	5-OH	386.57		96.36	183.21	448.86
	3′-OH	338.66		48.45	171.64	412.52
3	5-OH	363.10	511.88	96.72	163.59	445.01
	3′-OH	327.91		61.53	157.15	416.25
4	5-OH	383.90	536.39	93.00	184.10	445.29
	4′-OH	315.77		24.00	124.25	437.02
	3′-OH	339.57		48.67	167.99	417.08

BDE, Bond dissociation enthalpy; IP, ionization potential; PDE, proton dissociation enthalpy; PA, proton affinity; ETE, electron transfer enthalpy.

Compound 2 exhibited the smallest HOMO-LUMO Egap of all the compounds studied, measuring 3.860 eV, whereas compound 3 displayed the widest Egap at 3.912 eV. Parameters such as chemical hardness (η) and electronic chemical potential (µ) serve as valuable indicators for describing the stability, reactivity, and hardness of compounds. The reactivity indices were computed using equations 1-5, outlined in Table 3. Notably, compound 2 showed the lowest η value at 1.929 eV, while compound 3 presented the highest value at 1.956 eV. The results aligned with the LUMO-HOMO band gap trends observed across all compounds. Furthermore, compound 2 exhibited the highest µ value of -4.178 eV among the compounds, whereas compound 3 displayed the lowest µ value of -4.273 eV.

The computational thermochemical data for the compounds under investigation at the B3LYP level in water media (PCM) using the 6-311++G(d,p) basis set are outlined in Table 4. The presence of phenolic OH groups on the 5, 7, 4′, and 3′ positions of flavonoid ring contributed to their antioxidant properties. These compounds could yield 4 distinct phenoxide radicals through the cleavage of O-H bonds at positions C5, C7, C4′, and C3′. Compounds 2 and 4 exhibited 3 possible options for O-H bond cleavage, while compound 3 had 2 alternatives.

The formation of ArO• is crucial in all 3 mechanisms, including HAT, SPLET, and SET-PT. Therefore, irrespective of the particular mechanism involved, the radical scavenging or antioxidant effectiveness of flavonoids was associated with the stability of the generated radicals. To assess this, the dispersion of the unpaired electron in ArO• was analyzed in Fig. 3.

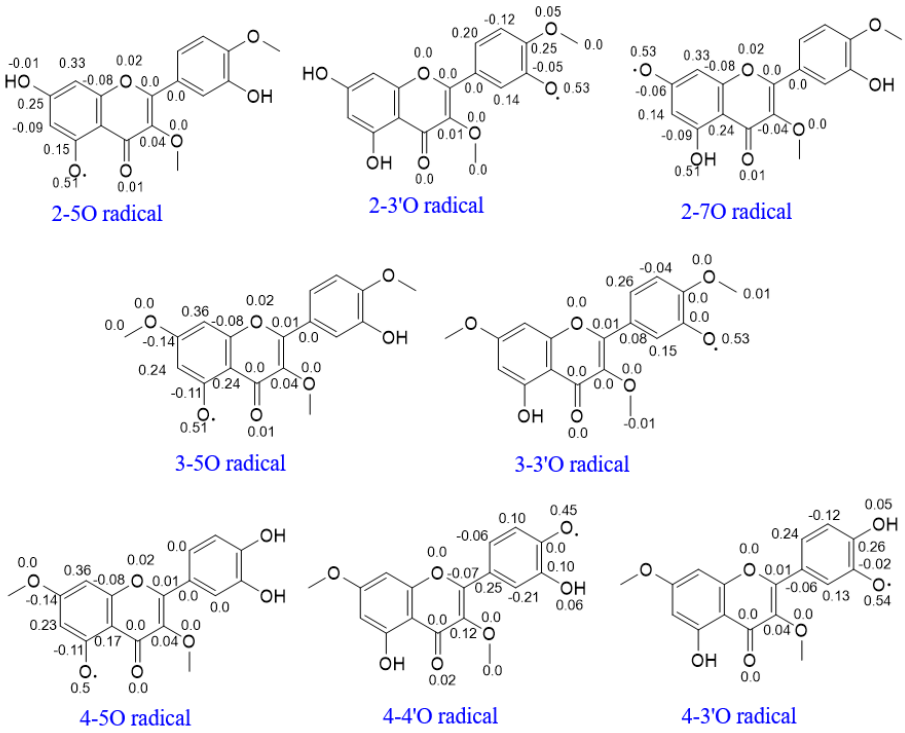

Fig. 3. The spin density distribution of the radical species of the structures studied. For computational simplification, all glycosidic subunits at C3 and C7 positions were replaced by methyl groups.

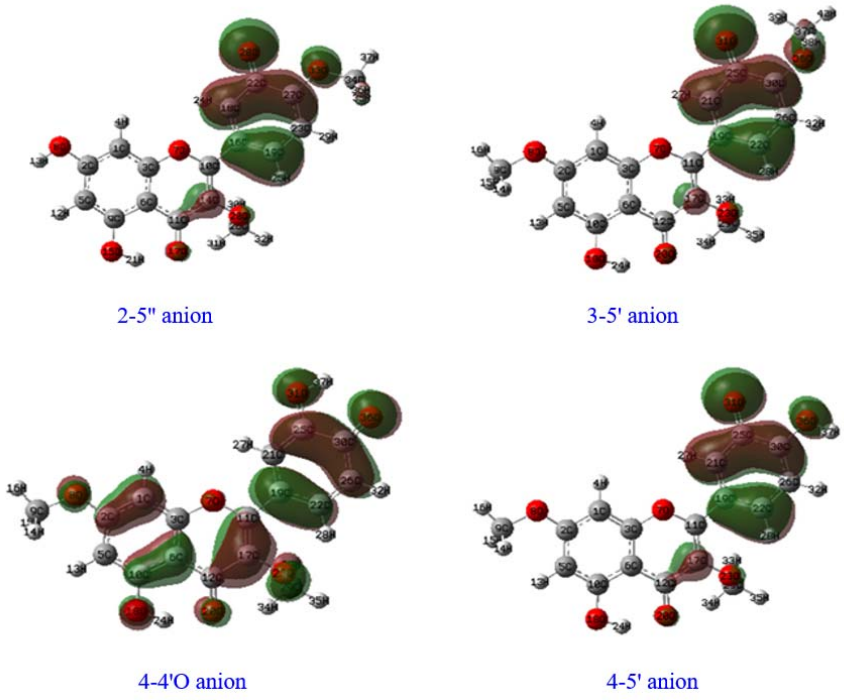

Fig. 4. Highest-occupied molecular orbital shapes of anion species of compounds studied. For computational simplification, all glycosidic subunits at C3 and C7 positions were replaced by methyl groups.

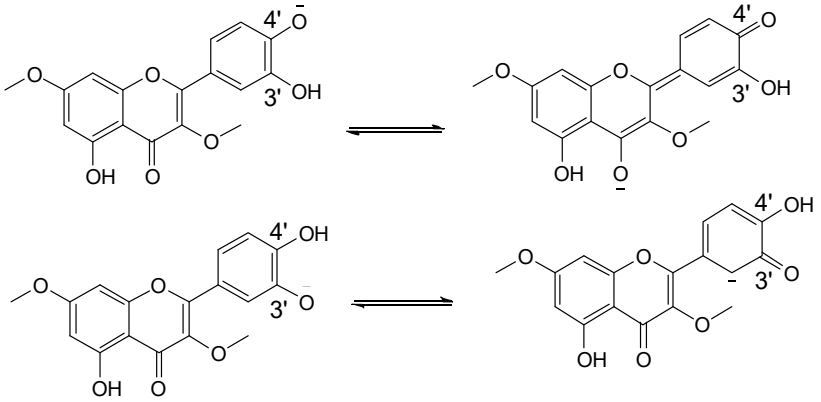

Fig. 5. Resonance of double bonds of anion species formed on C4' and C3' positions of flavonoids. For computational simplification, all glycosidic subunits at C3 and C7 positions were replaced by methyl groups.

The investigation of HOMO distribution of anion species of studied structures (Fig. 4) revealed that anion formation in C4' and C3' positions of the ring B of the flavonoid structure was preferred over other positions. Also, anion formation in C4'-O was more preferred than in C5-O. This observation was in accordance with the PDE values presented in Table 4. This phenomenon was explained by the fact that when the anion was formed at position C4', the double bonds were displaced, and the conjugation of these double bonds continued to ring A of the flavonoid structure (Fig. 5). Thus, this anionic structure would be more stable than the anion structure that formed on the C3' position.

DISCUSSION

Compound 1, with the experimental mass of 159 $[M+H]^+$ and NMR analysis, indicated allantoin, which agrees with the literature (29). Compound 2 was isolated as a light yellow solid and positively responded to a flavonoid natural product reagent (1% 2-aminoethyl diphenylborinate). The UV spectrum displayed absorption peaks at 257 and 355 nm, indicative of flavone derivative characteristics. Analysis of the NMR spectrum of the aglycone components revealed the presence of a single conjugated carbonyl carbon [ν max: 1657cm^{-1}; δ_C 177.8; C4], along with a signal at δ_H 12.62 ppm corresponding to a chelated hydroxyl group (5-OH). Additionally, meta-coupled doublets were observed at δ_H 6.20 (d, J = 2.0) and 6.44 (d, J = 2.0) representing H-6 and H-8, respectively. Ortho-coupled proton signals were noted at δ_H 6.91 (d, J = 8.4) and 7.48 (dd, J = 8.4, 2.0) corresponding to H-5' and H-6', as well as δ 7.94 (d, J = 2.0) associated with the H-2' proton. Following the acid hydrolysis of compound 2, the aqueous layer was isolated and subjected to TLC analysis, which was compared with standard sugars. Based on chemical shifts, the sugar was identified as glucose (30,31). Ultimately, according to HMBC correlations, compound 2 was identified as 4'-O-methylquercetin-3-O-β-D-glucopyranoside as reported by Chang *et al.* (32), which was further validated by the negative ion ESI showing peaks at 477 $[M-H]^-$, 447 $[M-MeO]^-$, and 315 $[M-Glucosyl]^-$ (Fig. 1). Compound 3 displayed a UV spectrum and aglycone NMR resonances similar to compound 2 but differed in having an additional 7-O-rhamnosyl moiety. This was evident in the NMR signals at δ_H 5.56 (broad singlet, rhamnosyl-H-1″), 5.59 (doublet, J = 7.8, Glucose-H-1″), 3.12-5.2 (overlapping signals from glucosyl H-2″-H-6″ and rhamnosyl H-2‴-H-5‴), and 1.11 (doublet, J = 6.4, rhamnosyl H-6‴), indicating the presence of one rhamnosyl and one glucosyl in the molecule. Compound 3 was identified as 4′-O-methylquercetin-3-O-β-D-glucopyranoside-7-O-α-L-rhamnopyranoside, which was confirmed by the negative ion ESI showing peaks at 623 $[M-H]^-$, 593 $[624-MeO]^-$, 477 $[624-rhamnosyl]^-$, and 316 $[M-glucosyl-rhamnosyl]^-$ as an undescribed compound. Its similar functional isomer, isorhamnetin-3-O-glucoside-7-O-rhamnoside, was reported

before from *Hippophaë rhamnoides* (33-35). Finally, the NMR resonances of compound 4 resembled those of compound 3, but without the methoxy group on C4′, and were identified as quercitin-3-O-β-D-glucopyranoside-7-O-α-L-rhamnopyranoside (36-38).

The phenolic hydroxyl group is prone to homolytic cleavage upon interaction with a radical such as DPPH•. Table 4 presents the BDE values for the homolytic cleavage of these O-H bonds, calculated using Equation 6 as previously outlined (26). Lower BDE values suggested higher antioxidant activity and implied the potential for a HAT antioxidant mechanism.

Typically, BDE values were lower in the ring B (C4′-OH and C3′-OH) than in the ring A (C5-OH and C7-OH) within the flavonoid structure. In compound 2, the most stable radical was formed by cleaving the C3′O-H bond in ring B, as it had the lowest BDE of 338.66 kJ/mol, contrasting with the BDE values for the C7O-H (362.72 kJ/mol) and C5O-H (386.57 kJ/mol) bonds. Similarly, for compounds 3 and 4, the easiest O-H bond cleavage occurred at the C4′ and C3′ positions in ring B.

It is noteworthy that among the 4 types of hydroxyl groups in the analyzed structures, C4′-OH in the ring B of the flavonoid system (as depicted in Fig. 1) exhibited the lowest BDE value, indicating its superior capability to donate an H-atom during homolytic O-H bond cleavage. Consequently, C4′-OH was identified as the primary site for potential H-atom donation.

These data agree with the obtained experimental EC_{50} of the DPPH scavenging assay (Table 1). Compound 4 exhibited the most scavenging activity among all the compounds because it contained 2 OH groups at C4′ and C3′ in ring B.

In SET-PT, an electron is moved from the antioxidant to the free radical, creating a radical cation that subsequently loses a proton. Therefore, IP and PDE are crucial factors in elucidating the plausibility of SET-PT.

The IP for the cleavage of the O-H bond was determined using equation 7 (26). As indicated in Table 4, the IP values for the studied compounds followed the order 4, 2, and 3, suggesting a preference for ionization of the neutral form of compound 3. Generally, a lower IP indicates a higher likelihood of ionization and facilitates the transfer of electrons between free radicals and antioxidants. Based on this criterion, the probability of radical cation formation from the neutral form was the highest, while the formation of a radical cation in compound 4 was less probable. However, the IP results do not align with the experimental findings presented in this study.

In the subsequent stage of the mechanism, the significant parameter, PDE, gauged the propensity for deprotonation of the radical cations generated in the first step. PDE was derived from the enthalpies of the heterolytic O-H bond cleavage according to equation 8 (26). As demonstrated in Table 4, the lowest PDE was observed for C4′-OH in molecule 4, indicating a greater inclination towards deprotonation in all the structures investigated. Additionally, the PDE values were lower in the ring B(C4′-OH and C3′-OH) compared to the ring A(C5-OH and C7-OH). Consequently, the PDE results are consistent with the experimental data. Compound 4 displayed the highest scavenging activity among the compounds due to its possessing 2 OH groups with lower PDE and a heightened propensity for deprotonation at C4′-OH and C3′-OH in ring B.

An alternative pathway for capturing radicals, particularly in polar environments, is through SPLET. Foti *et al*. proposed SPLET as a potential mechanism for trapping the DPPH free radical using flavonoids in polar solvents like methanol. Their study suggested that flavonoids initially underwent proton loss from the corresponding anion form (ArO-) in ionizing solvents. Subsequently, in the second step, the anion transferred an electron to the DPPH free radical, resulting in the formation of ArO• (39).

The PA and ETE values of the compounds under investigation, calculated using equations 9 and 10 (26), were presented in Table 4. The first step of the SPLET mechanism required more energy than the second step, indicating that the first step was the slowest and rate-determining step. PA signified the index for the first step, while ETA described the second step

of the potential SPLET mechanism. Among all the OH groups in the studied compounds, C4′-OH in ring B (molecule 4) and C7-OH in ring A (molecule 2) exhibited the lowest PA values, suggesting a higher likelihood of proton transfer from these OH groups.

The data in Table 4 also displayed ETE values for the anion species at potential OH positions in a water environment (PCM) for the studied compounds. These values suggested that releasing an electron from the anion form in C3′-OH of ring B, among all the structures studied, was slightly more favorable than others, while the generation of radicals in C5-OH of ring A was unlikely. These values correlated logically with the experimental EC50 values (Table 2) of the DPPH scavenging assay.

In general, the studied compounds exhibited PA values lower than their corresponding BDE and IP values, suggesting that SPLET is the most likely reaction pathway from a thermodynamic standpoint in a water environment. Conversely, the high BDE values indicated that HAT was not the preferred mechanism for these molecules in aqueous media. These results are consistent with the findings of Foti's study, who advocated for the SPLET mechanism in the interaction of DPPH with flavonoids and quercetin in polar solvents and concluded that HAT is thermodynamically favored in the gaseous media (39). A comparison of electronic descriptors, reactivity indices, and experimental DPPH scavenging outcomes showed that these compounds can donate electrons to free radicals instead of capturing them, showing their antioxidant properties (39).

A decrease in spin density at the oxygen atom of ArO• typically signified an improvement in radical scavenging effectiveness. As depicted in Fig. 3, the spin density predominantly resided on the oxygen atom in the C4′-O• radical, resulting in relatively limited electron delocalization in ring A (C5 and C7-O•) compared to ring B (C4′ and C3′-O•). This localization enhanced the stability of the C4′-O• radical, thereby reducing the bond dissociation energy of the C4′-OH group.

In the context of the Fenton reaction, OH radicals were produced from H2O2 in the presence of metal ions like ferrous ($Fe^{2+} + H_2O_2 \rightarrow Fe^{3+} + OH^- + OH^•$). Flavonoids can chelate Fe^{2+}, Fe^{3+}, and Cu^{2+} ions and quench their related metal-catalyzed free radical production. In this way, they show an antioxidant capacity.

Consequently, a lower PA value indicated easier deprotonation and metal chelation. Based on the PA values obtained (Table 4), it is evident that C4′-OH in ring B and C7-OH in ring A exhibited the lowest PA values, suggesting higher reactivity in interactions with metal ions in aqueous environments. These data are in agreement with the results for reducing power activity. According to the presented EC_{50} value for the reducing power activity (Table 2), compound 4 exhibited the highest reducing power among all the studied structures. It can be related to the lowest PA value at the C4′-OH position and its catechol structure because of the neighborhood of the hydroxyl group, which causes the formation of a bidentate ligand and the formation of more stable hexagonal chelation rings.

This study agrees with other studies on the in vitro antioxidant activity of quercetin and its derivatives. Quercetin acts as an antioxidant in vitro by neutralizing free radicals and protecting human keratinocytes from hydrogen peroxide damage. It chelates metal ions such as Cu^{2+} and Fe^{2+}, which helps reduce oxidative damage by inhibiting Fe^{2+}-induced lipid peroxidation and preventing iron overload, especially in alcoholic liver disease (40). Additionally, quercetin prevents oxidative modification of low-density lipoprotein (LDL) and increases LDL receptor expression, thereby minimizing LDL oxidative damage (41). In the *in vivo* systems, the antioxidant mechanism of quercetin is somewhat different. It primarily involves regulating glutathione levels to boost antioxidant capacity. It facilitates the conversion of superoxide (O^{2-}) to hydrogen peroxide (H_2O_2) *via* superoxide dismutase 2, and glutathione peroxidase, then breaks down H_2O_2 into water, relying on glutathione for reducing hydrogen (42). Quercetin enhances the expression of antioxidant enzymes like glutathione transferase and aldo-keto reductase, with levels increasing in proportion to quercetin

intake (42). It also upregulates genes associated with oxidative stress *in vivo* and *in vitro*, providing protective effects on granulosa cells (43).

In addition, this study investigated the mechanisms of the antioxidant effect using DFT calculations. In addition to confirming the laboratory effects, this computational and theoretical approach helps to analyze the electronic structure of the desired compounds and provide detailed insight into their reactivity and various interactions, including hydrogen, hydrophobic, and van der Waals bonds at the molecular level. This allows researchers to find out how these compounds transfer electrons or hydrogen atoms and ultimately neutralize ROS or free radicals (44,45).

CONCLUSION

In conclusion, allantoin and 3 known flavonol glycosides were isolated from *C. turkmena* Bobrov. Compounds 2, 3, and 4 demonstrated strong ferric reduction power and high scavenging activity against DPPH free radicals. Both methodologies indicated that the 4′-OH group was the most favorable site for homolytic and heterolytic O-H bond cleavage in an aqueous environment, while the 5-OH group was not preferred for neutralizing radicals. In aqueous conditions, the SPLET mechanism appears to be the energetically favored reaction pathway, with the PA of the OH groups significantly lower than their corresponding BDEs and IPs. This research underscores the potential utility of DFT (B3LYP) methods in exploring the energetic aspects of free radical scavenging by flavonoids. Ultimately, it concluded that flavonoids exhibited stronger antioxidant effects when they contain: a. more phenolic OH groups in their structures; b. phenolic OH substituents at the C4′ and C7 positions; and c. substitutions on the ring B that increase conjugated double bonds, facilitating electron density delocalization.

Acknowledgments

This work was supported by the Pharmaceutical Sciences Research Center of the School of Pharmacy and Pharmaceutical Sciences of Isfahan University of Medical Sciences, Isfahan, Iran. Special thanks to Prof. Ebrahim Sajjadi, who supported us with his mentorship, assistance, and insightful guidance throughout this research. Also, we especially appreciate Dr. Mohammad Reza Joharchi, who helped us to identify *Cleome turkmena* Bobrov correctly.

Conflict of interest statement

All authors declared no conflict of interest in this study.

Authors' contributions

M. Ghanadian, E. Elahi, and S. Abdeyazdan conceived, designed, extracted, and identified the compounds of plant materials and measured antioxidant activity; M. Ghanadian, M. Mohammadpour Dehkordi, and S. Mousavi participated in the theoretical calculations, analyzed the data, and wrote the manuscript. All authors have read and approved the finalized article. Each author has fulfilled the authorship criteria and affirmed that this article represents honest and original work.

AI declaration

During the preparation of this work, the authors used Grammarly AI to improve readability and language. After using this tool, the authors reviewed and edited the content and take full responsibility for the content of the publication.

REFERENCES

1. Karimi H. A dictionary of Iran's vegetation plants. Tehran: Parcham Publisher; 2002. pp. 3-6.
2. Adhikari PP, Paul SB. Medicinally important plant *Cleome gynandra*: a phytochemical and pharmacological explanation. Asian J Pharm Clin Res. 2018;11(1):21-29. DOI: 10.22159/ajpcr.2018.v11i1.22037.
3. Chand J, Panda SR, Jain S, Murty USN, Das AM, Kumar GJ, *et al*. Phytochemistry and polypharmacology of *cleome* species: a comprehensive Ethnopharmacological review of the medicinal plants. J Ethnopharmacol. 2022;282:114600. DOI: 10.1016/j.jep.2021.114600.
4. Mali RG. *Cleome viscosa* (wild mustard): a review on ethnobotany, phytochemistry, and pharmacology. Pharm Biol. 2010;48(1):105-112. DOI: 10.3109/13880200903114209.
5. Jinazali H, Mtimuni B, Chilembwe E. Nutrient composition of cat's whiskers (*Cleome gynandra* L.)

from different agro ecological zones in Malawi. Afr J Food Sci. 2017;11(1):24-29.
DOI: 10.5897/AJFS2016.1478.
6. Abdel Motaal A, Salem HH, Almaghaslah D, Alsayari A, Bin Muhsinah A, Alfaifi MY,*et al*. Flavonol glycosides: *in vitro* inhibition of DPPIV, aldose reductase and combating oxidative stress are potential mechanisms for mediating the antidiabetic activity of *Cleome droserifolia*. Molecules. 2020;25(24):5864,1-13.
DOI: 10.3390/molecules25245864
7. Singh H, Mishra A, Mishra AK. The chemistry and pharmacology of *Cleome genus*: a review. Biomed Pharmacother. 2018;101:37-48.
DOI: 10.1016/j.biopha.2018.02.053.
8. Moyo M, Amoo SO, Aremu AO, Gruz J, Šubrtová M, Jarošová M, *et al*. Determination of mineral constituents, phytochemicals and antioxidant qualities of *Cleome gynandra*, compared to *Brassica oleracea* and *Beta vulgaris*. Front Chem. 2018;5:128,1-9.
DOI: 10.3389/fchem.2017.00128.
9. Nguyen TP, Tran CL, Vuong CH, Do THT, Le TD, Mai DT, *et al*. Flavonoids with hepatoprotective activity from the leaves of *Cleome viscosa* L. Nat Prod Res. 2017;31(22):2587-2592.
DOI: 10.1080/14786419.2017.1283497.
10. Aboushoer MI, Fathy HM, Abdel-Kader MS, Goetz G, Omar AA. Terpenes and flavonoids from an Egyptian collection of *Cleome droserifolia*. Nat Prod Res. 2010;24(7):687-696.
DOI: 10.1080/14786410903292433.
11. Xiao J. Dietary flavonoid aglycones and their glycosides: which show better biological significance? Crit Rev Food Sci Nutr. 2017;57(9):1874-1905.
DOI: 10.1080/10408398.2015.1032400.
12. Hollman PCH, Geelen A, Kromhout D. Dietary flavonol intake may lower stroke risk in men and women. J Nutr. 2010;140(3):600-604.
DOI: 10.3945/jn.109.116632.
13. Calderón-Montaño JM, Burgos-Morón E, Pérez-Guerrero C, López-Lázaro M. A review on the dietary flavonoid kaempferol. Mini Rev Med Chem. 2011;11(4):298-344.
DOI: 10.2174/138955711795305335.
14. Cizmarova B, Hubkova B, Birkova A. Quercetin as an effective antioxidant against superoxide radical. Funct Food Sci. 2023;3(3):15-25.
DOI: 10.31989/ffs.v3i3.1076.
15. Shahbaz M, Imran M, Alsagaby SA, Naeem H, Al Abdulmonem W, Hussain M, *et al*. Anticancer, antioxidant, ameliorative and therapeutic properties of kaempferol. Int J Food Prop. 2023;26(1):1140-1166.
DOI: 10.1080/10942912.2023.2205040.
16. Agraharam G, Girigoswami A, Girigoswami K. Myricetin: a multifunctional flavonol in biomedicine. Curr Pharmacol Rep. 2022;8(1):48-61.
DOI: 10.1007/s40495-021-00269-2.
17. Marnett LJ. Oxyradicals and DNA damage. Carcinogenesis. 2000;21(3):361-370.
DOI: 10.1093/carcin/21.3.361.
18. Bartolotti LJ, Flurchick K. An introduction to density functional theory. In: Lipkowitz KB, Boyd DB, editors. Reviews in computational chemistry. Vol 7. New York: Wiley-VCH, Inc., 1996. pp. 187-216.
DOI: 10.1002/9780470125847.ch4.
19. Mahmoudi S, Mohammadpour Dehkordi M, Asgarshamsi MH. Density functional theory studies of the antioxidants- a review. J Mol Model. 2021;27(9):271,1-14.
DOI: 10.1007/s00894-021-04891-1.
20. Fassihi A, Hasanzadeh F, Movahedian Attar A, Saghaie L, Mohammadpour M. Synthesis and evaluation of antioxidant activity of some novel hydroxypyridinone derivatives: a DFT approach for explanation of their radical scavenging activity. Res Pharm Sci. 2020;15(6):515-528.
DOI: 10.4103/1735-5362.301336.
21. Nazifi SMR, Asgharshamsi MH, Dehkordi MM, Zborowski KK. Antioxidant properties of *Aloe vera* components: a DFT theoretical evaluation. Free Radic Res. 2019;53(8):922-931.
DOI: 10.1080/10715762.2019.1648798.
22. Khuntia A, Martorell M, Ilango K, Bungau SG, Radu AF, Behl T, *et al*. Theoretical evaluation of *Cleome* species' bioactive compounds and therapeutic potential: a literature review. Biomed Pharmacother. 2022;151:113161.
DOI: 10.1016/j.biopha.2022.113161.
23. Abdullah W, Elsayed WM, Abdelshafeek KA, Nazif NM, Singab ANB. Chemical constituents and biological activities of *Cleome* genus: a brief review. Int J Pharmacogn Phytochem Res. 2016;8(5):777-787.
24. Pasdaran A, Delazar A, Ayatollahi SA, Pasdaran A. Chemical composition and biological activities of methanolic extract of *Scrophularia oxysepala* Boiss. Iran J Pharm Res. 2017;16(1):338-346.
PMID: 28496487.
25. Salmanian S, Sadeghi Mahoonak AR, Alami M, Ghorbani M. Phenolic content, antiradical, antioxidant, and antibacterial properties of hawthorn (*Crataegus elbursensis*) seed and pulp extract. J Agr Sci Tech. 2014;16(2):343-354.
26. Dehkordi MM, Asgarshamsi MH, Fassihi A, Zborowski KK. A comparative DFT study on the antioxidant activity of some novel 3-hydroxypyridine-4-one derivatives. Chem Biodiver. 2022;19(3):e202100703.
DOI: 10.1002/cbdv.202100703.
27. Mittal A, Kakkar R. The effect of solvent polarity on the antioxidant potential of echinatin, a retrochalcone, toward various ROS: a DFT thermodynamic study. Free Radic Res. 2020;54(10):777-786.
DOI: 10.1080/10715762.2020.1849670.
28. Chen Z, Bertin R, Froldi G. EC50 estimation of antioxidant activity in DPPH· assay using several statistical programs. Food Chem. 2013;138(1):414-420.
DOI: 10.1016/j.foodchem.2012.11.001.
29. Liu S, Liu M, Wu H, Wang Q, Li W, Huang S, *et al*. A new isomer and other metabolites isolated from

Alternaria alternata. Chem Nat Compd. 2021;57:844-847.
DOI: 10.1007/s10600-021-03495-8.
30. Foo LY, Lu Y, Molan AL, Woodfield DR, McNabb WC. The phenols and prodelphinidins of white clover flowers. Phytochemistry. 2000;54(5):539-548.
DOI: 10.1016/S0031-9422(00)00124-2.
31. Chawla R, Arora R, Sagar RK, Singh S, Puri SC, Kumar R, *et al*. 3-O-beta-D-Galactopyranoside of quercetin as an active principle from high altitude *Podophyllum hexandrum* and evaluation of its radioprotective properties. Z Naturforsch C J Biosci. 2005;60(9-10):728-738.
DOI: 10.1515/znc-2005-9-1012.
32. Chang L, Shao Q, Xi X, Chu Q, Wei Y. Separation of four flavonol glycosides from *Solanum rostratum* Dunal using aqueous two-phase flotation followed by preparative high-performance liquid chromatography. J Sep Sci. 2017;40(3):804-812.
DOI: 10.1002/jssc.201600922.
33. Yang B, Halttunen T, Raimo O, Price K, Kallio H. Flavonol glycosides in wild and cultivated berries of three major subspecies of *Hippophaë rhamnoides* and changes during harvesting period. Food Chem. 2009;115(2):657-664.
DOI: 10.1016/j.foodchem.2008.12.073.
34. Rösch D, Krumbein A, Mügge C, Kroh LW. Structural investigations of flavonol glycosides from sea buckthorn (*Hippophaë rhamnoides*) pomace by NMR spectroscopy and HPLC-ESI-MS(n). J Agric Food Chem. 2004;52(13):4039-4046.
DOI: 10.1021/jf0306791.
35. Fang R, Veitch NC, Kite GC, Porter EA, Simmonds MSJ. Enhanced profiling of flavonol glycosides in the fruits of sea buckthorn (*Hippophae rhamnoides*). J Agric Food Chem. 2013;61(16): 3868-3875.
DOI: 10.1021/jf304604v.
36. Medjahed Z, Chaher-Bazizi N, Atmani-Kilani D, Ahmane N, Ruiz-Larrea MB, Sanz JIR, *et al*. A novel flavonol glycoside and six derivatives of quercetin and kaempferol from *Clematis flammula* with antioxidant and anticancer potentials. Fitoterapia. 2023;170:105642.
DOI: 10.1016/j.fitote.2023.105642.
37. Alaniya MD, Sutiashvili MG, Skhirtladze AV, Getia MZ, Jgerenaia GA, Mskhiladze LV. Phenolic compounds from aerial parts of *Ononis arvensis*. Chem Nat Compd. 2023;59:783-784.
DOI: 10.1007/s10600-023-04111-7
38. Wang X, Yu R. Chemical compositions of *Lepidium latifolium*. Chem Nat Compd. 2024;60(1).
DOI: 10.1007/s10600-024-04276-9.
39. Foti MC. Antioxidant properties of phenols. J Pharm Pharmacol. 2007;59(12):1673-1685.
DOI: 10.1211/jpp.59.12.0010.
40. Yang D, Wang T, Long M, Li P. Quercetin: its main pharmacological activity and potential application in clinical medicine. Oxid Med Cell Longev. 2020;2020:8825387,1-13.
DOI: 10.1155/2020/8825387.
41. Mbikay M, Sirois F, Simoes S, Mayne J, Chrétien M. Quercetin-3-glucoside increases low-density lipoprotein receptor (LDLR) expression, attenuates proprotein convertase subtilisin/kexin 9 (PCSK9) secretion, and stimulates LDL uptake by Huh7 human hepatocytes in culture. FEBS Open Bio. 2014;4:755-762.
DOI: 10.1016/j.fob.2014.08.003.
42. Odbayar TO, Kimura T, Tsushida T, Ide T. Isoenzyme-specific up-regulation of glutathione transferase and aldo-keto reductase mRNA expression by dietary quercetin in rat liver. Mol Cell Biochem. 2009;325(1-2):121-130.
DOI: 10.1007/s11010-009-0026-4.
43. Wang J, Qian X, Gao Q, Lv C, Xu J, Jin H, *et al*. Quercetin increases the antioxidant capacity of the ovary in menopausal rats and in ovarian granulosa cell culture *in vitro*. J Ovarian Res. 2018;11(1): 51,1-11.
DOI: 10.1186/s13048-018-0421-0.
44. Asgarshamsi MH, Fassihi A, Hassanzadeh F, Saghaei L, Movahedian Attar A, Mohammad-Beigi H. Synthesis, antioxidant activity, and density functional theory study of some novel 4-[(benzo [d] thiazol-2-ylimino) methyl] phenol derivatives: a comparative approach for the explanation of their radical scavenging activities. Res Pharm Sci. 2020;16(1):35-47.
DOI: 10.4103/1735-5362.305187.
45. Mohammadpour M, Sadeghi A, Fassihi A, Saghaei L, Movahedian A, Rostami M. Synthesis and antioxidant evaluation of some novel ortho-hydroxypyridine-4-one iron chelators. Res Pharm Sci. 2012;7(3):171-179.
PMID: 23181095.